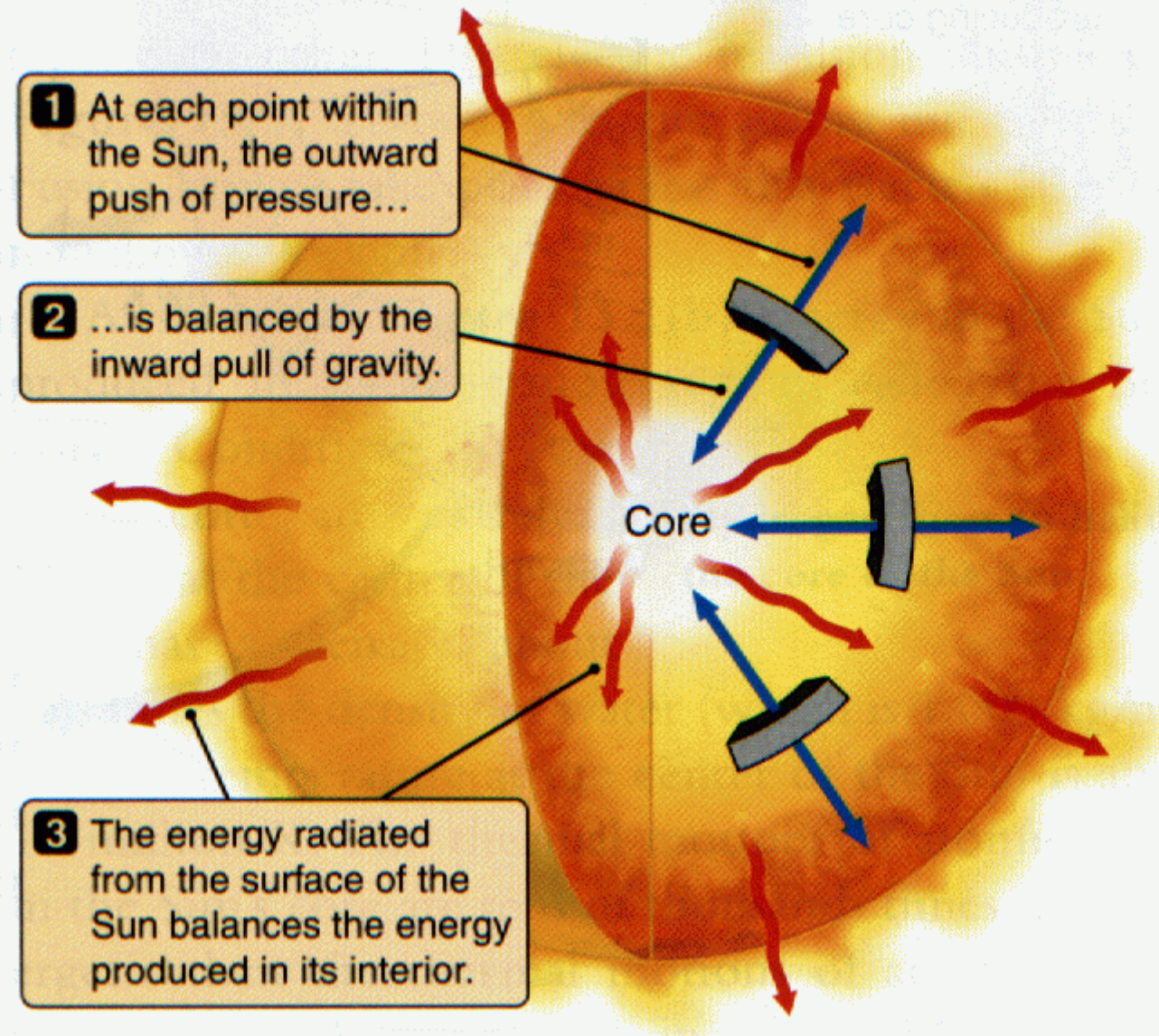
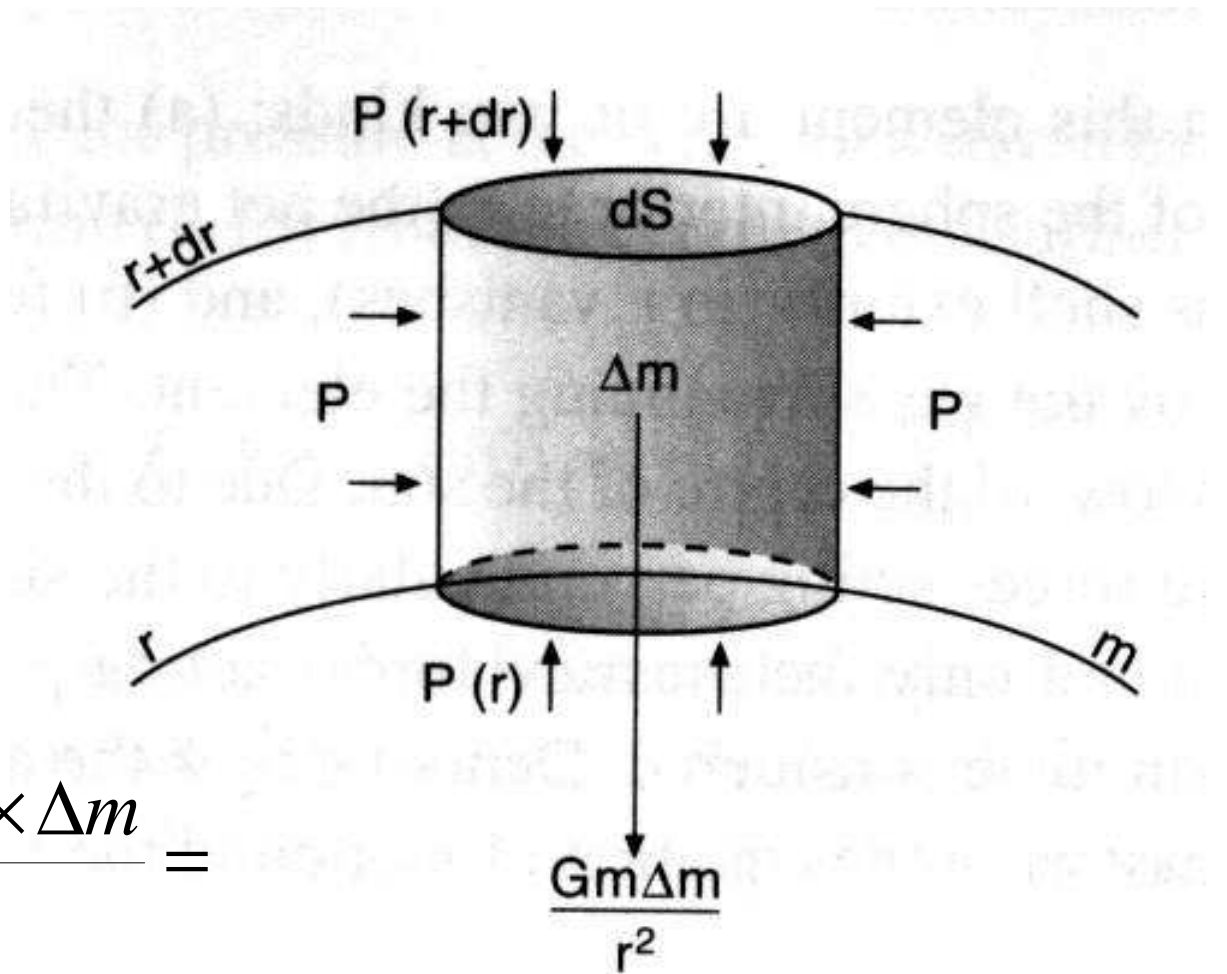


ESTRUCTURA

Figure 13.1 *The structure of the Sun is determined by balances between forces and in the outward flow of energy.*



ECUACION DE EQUILIBRIO HIDROSTATICO



$$\Delta P \times dS = -G \frac{M(r) \times \Delta m}{r^2} =$$

$$-G \frac{M(r) \times \rho \times dS \times dr}{r^2}$$

$$dP = -G \frac{M(r) \times \rho \times dr}{r^2}$$

$$dP = -G \frac{M(r) \times \rho \times dr}{r^2}$$

Si suponemos densidad constante:

$$dP = -G \frac{\frac{4}{3} \pi r^3 \rho \times \rho \times dr}{r^2}$$

$$\Rightarrow dP = -G \frac{4}{3} \pi \times r \times \rho^2 \times dr$$

$$P_{Sup} - P_{Centro} = -G \frac{4}{3} \pi \times \rho^2 \times \frac{R^2}{2}$$

Quién soporta esta presión?

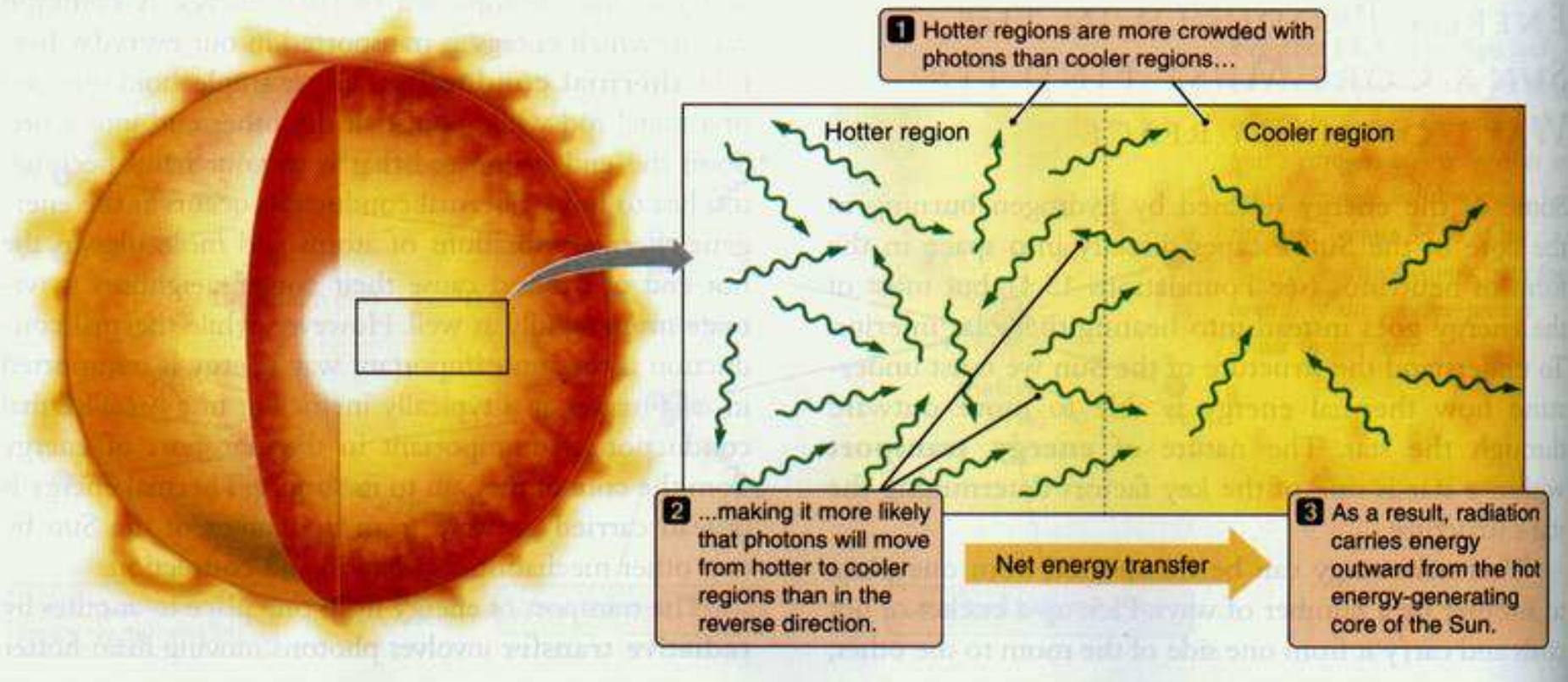
- Presión del gas (peso molecular medio)
- Presión de radiación (fotones)
- Presión de gas degenerado (electrones)

Stellar theory^a

Conservation of mass	$\frac{dM_r}{dr} = 4\pi\rho r^2$	(9.60)	r radial distance M_r mass interior to r ρ mass density
Hydrostatic equilibrium	$\frac{dp}{dr} = \frac{-G\rho M_r}{r^2}$	(9.61)	p pressure G constant of gravitation
Energy release	$\frac{dL_r}{dr} = 4\pi\rho r^2\epsilon$	(9.62)	L_r luminosity interior to r ϵ power generated per unit mass
Radiative transport	$\frac{dT}{dr} = \frac{-3}{16\sigma} \frac{\langle\kappa\rangle\rho}{T^3} \frac{L_r}{4\pi r^2}$	(9.63)	T temperature σ Stefan–Boltzmann constant $\langle\kappa\rangle$ mean opacity
Convective transport	$\frac{dT}{dr} = \frac{\gamma-1}{\gamma} \frac{T}{p} \frac{dp}{dr}$	(9.64)	γ ratio of heat capacities, c_p/c_v

^aFor stars in static equilibrium with adiabatic convection. Note that ρ is a function of r . κ and ϵ are functions of temperature and composition.

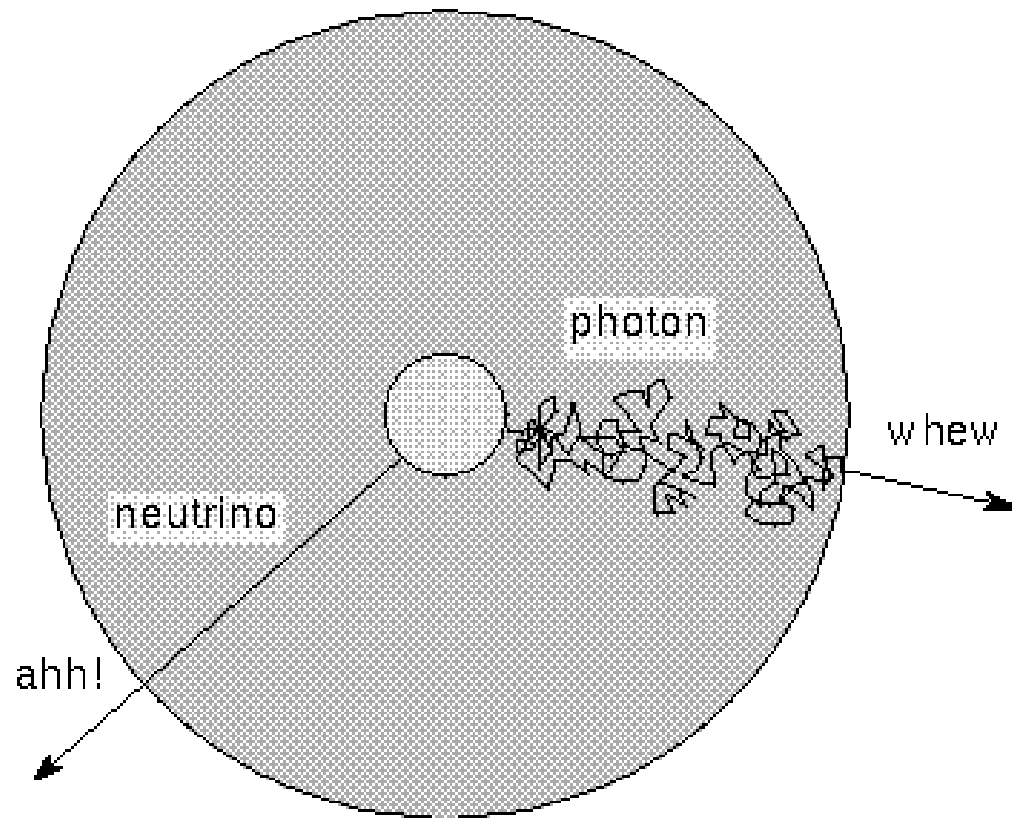
Figure 13.5 Higher-temperature regions deep within the Sun produce more radiation than lower-temperature regions farther out. While radiation flows in both directions, more radiation flows from the hot regions to the cooler regions than from the cooler regions to the hot regions. In this way, radiation carries energy outward from the inner parts of the Sun.



transformacion gamma - visible

$$CLM = \frac{1}{\kappa \rho} = \frac{1}{\alpha}$$

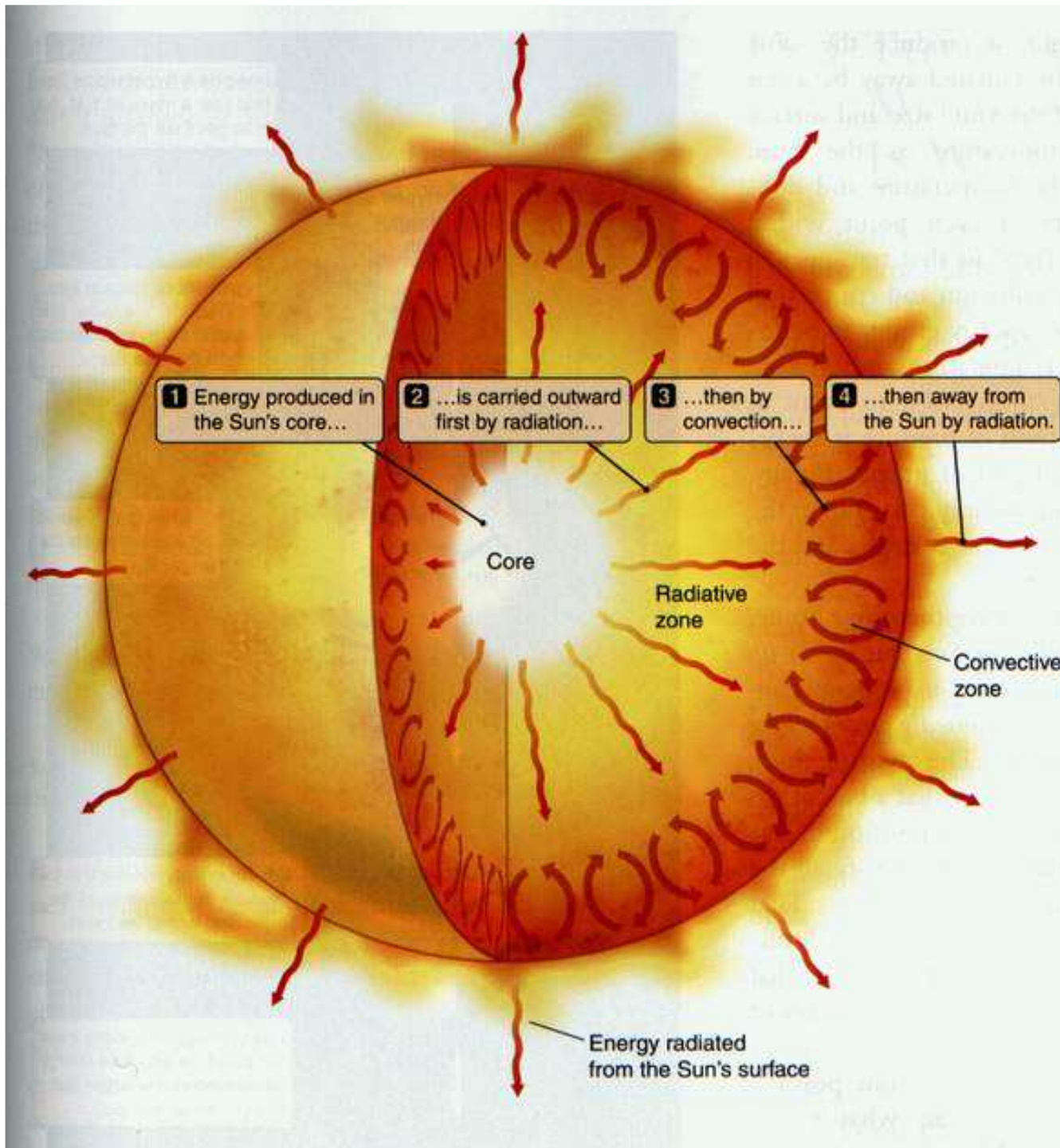
La OPACIDAD del medio es una medida de la dificultad que experimenta la radiación (fotones) en atravesarlo



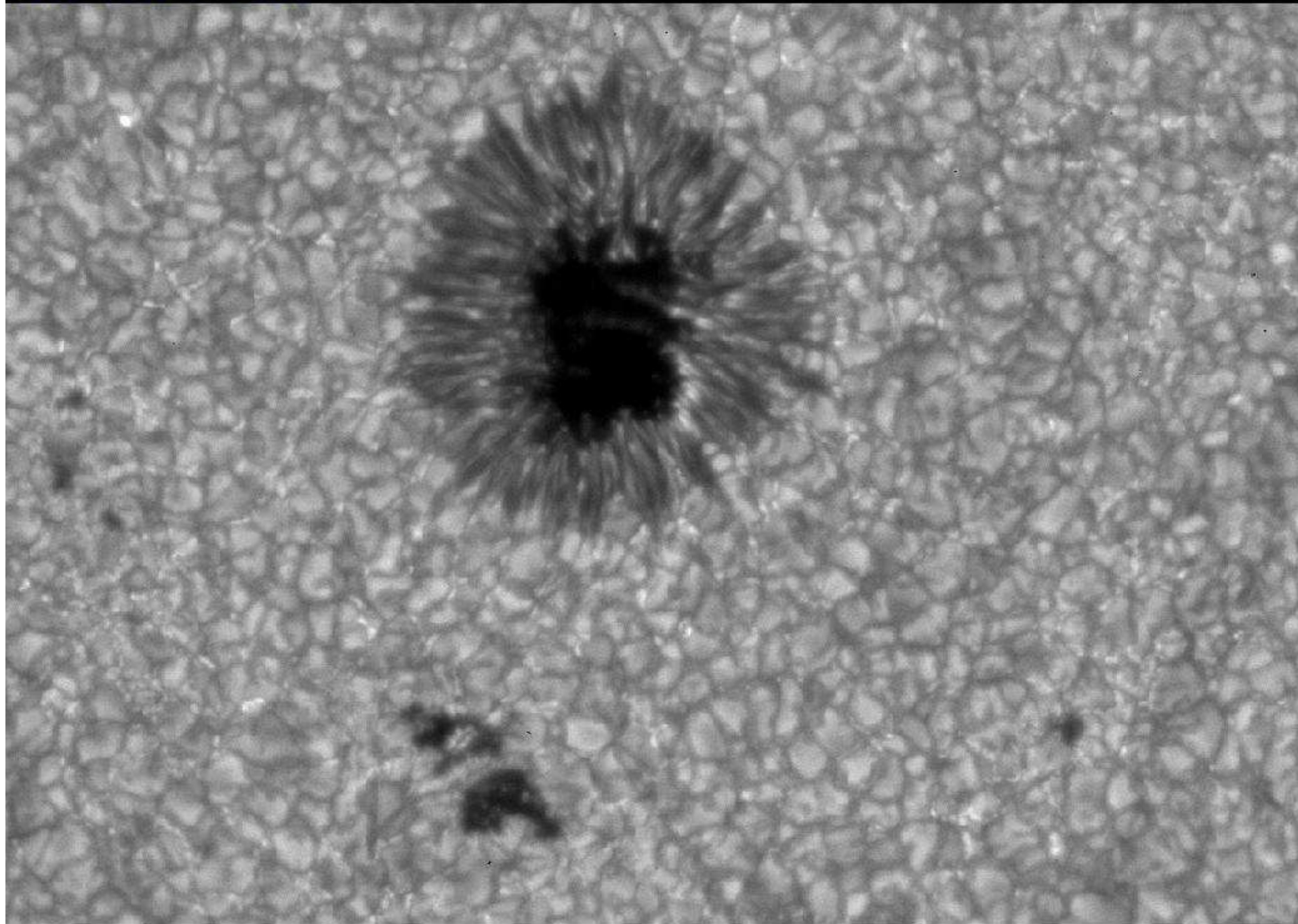
Photons take tortuous paths out of the Sun's interior. Neutrinos pass right on through in just two seconds.

Figure 13.6 The interior structure of the Sun is divided into zones on the basis of where energy is produced and how it is transported outward.

SOL



June 1994: G-Band



cc: Kienapheuer/Hensals/Lockheed (P. Brandt, C. Simon, C. Schermer, P. Shino)

HAC A-

Rotacion diferencial y actividad solar

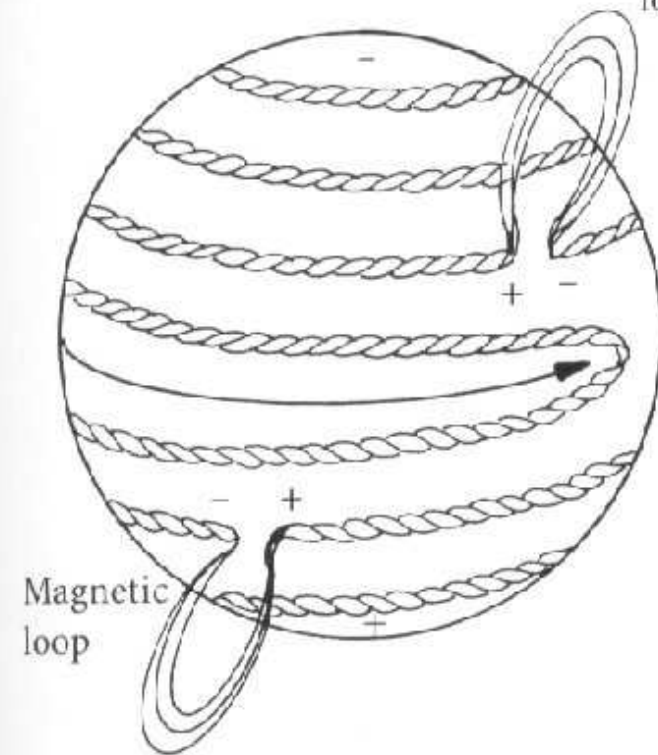
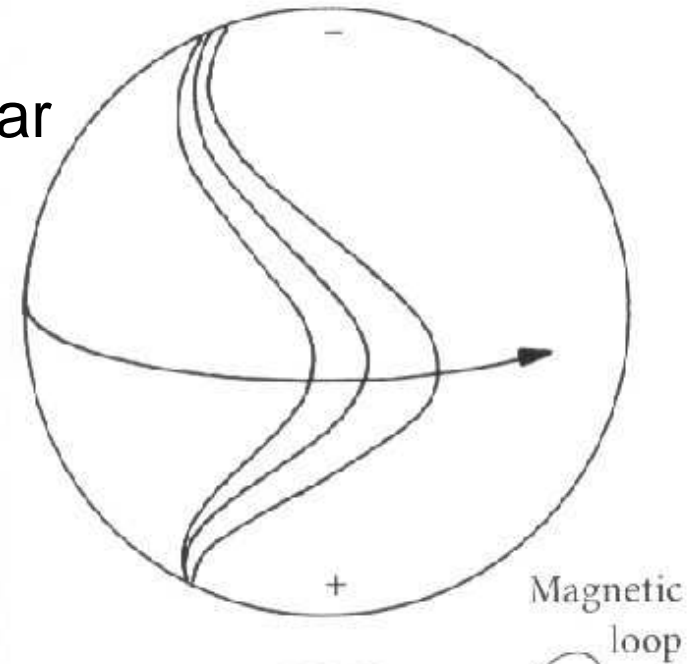
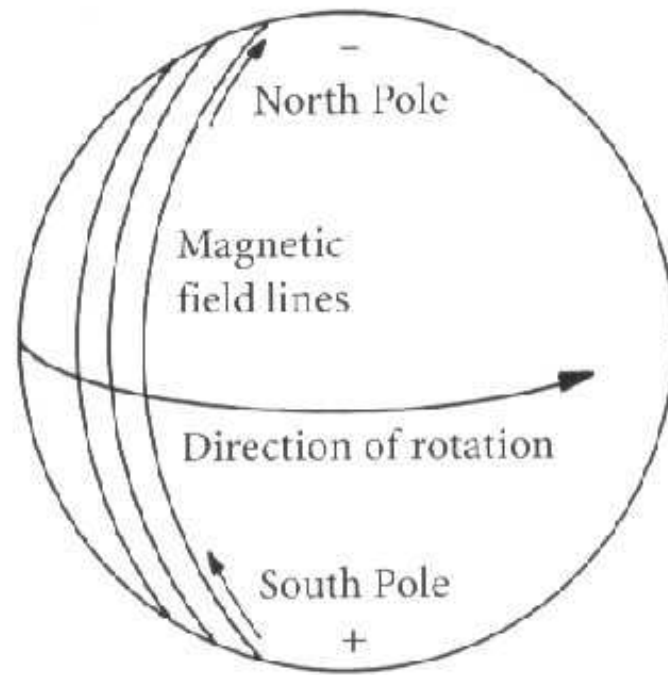
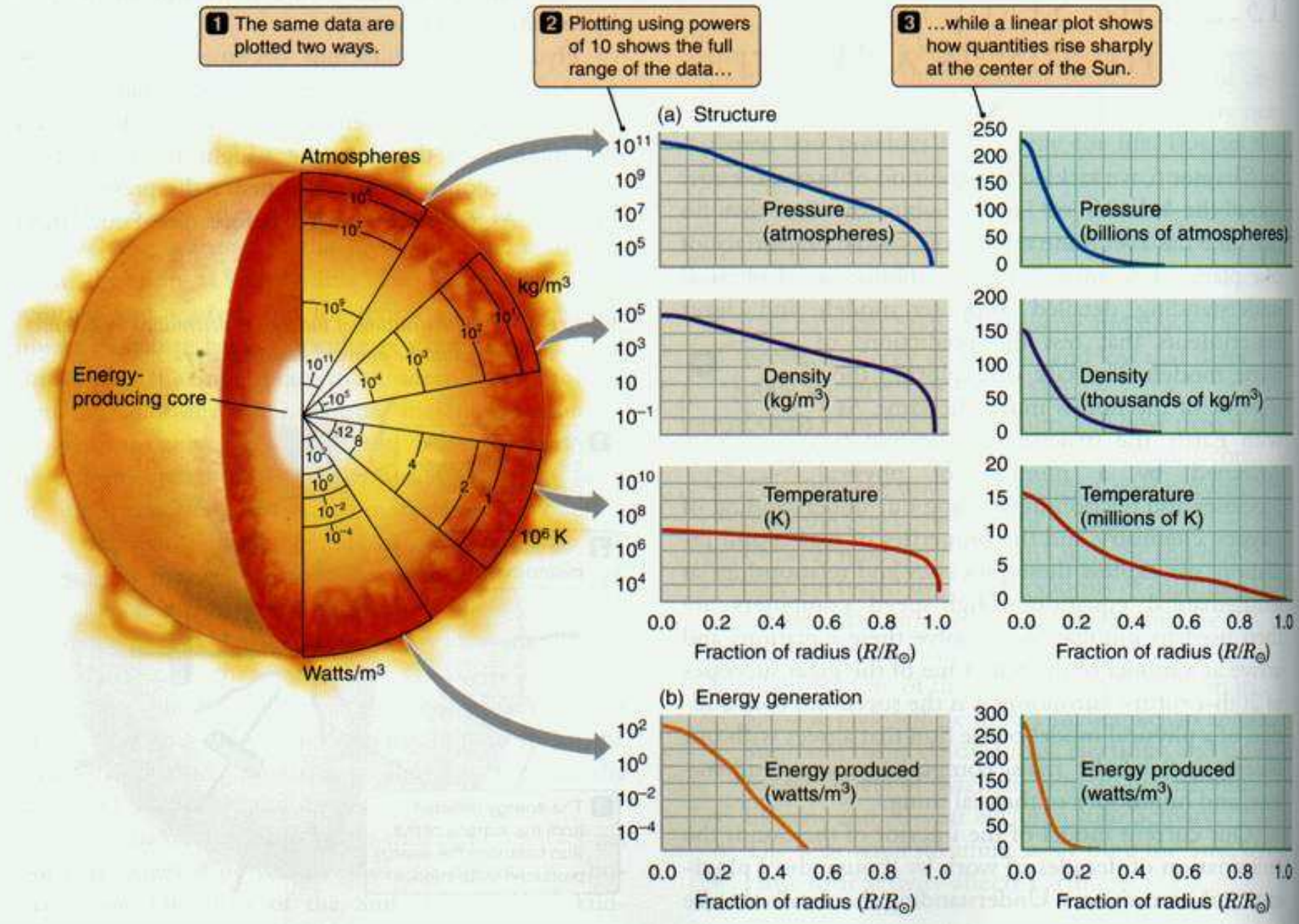
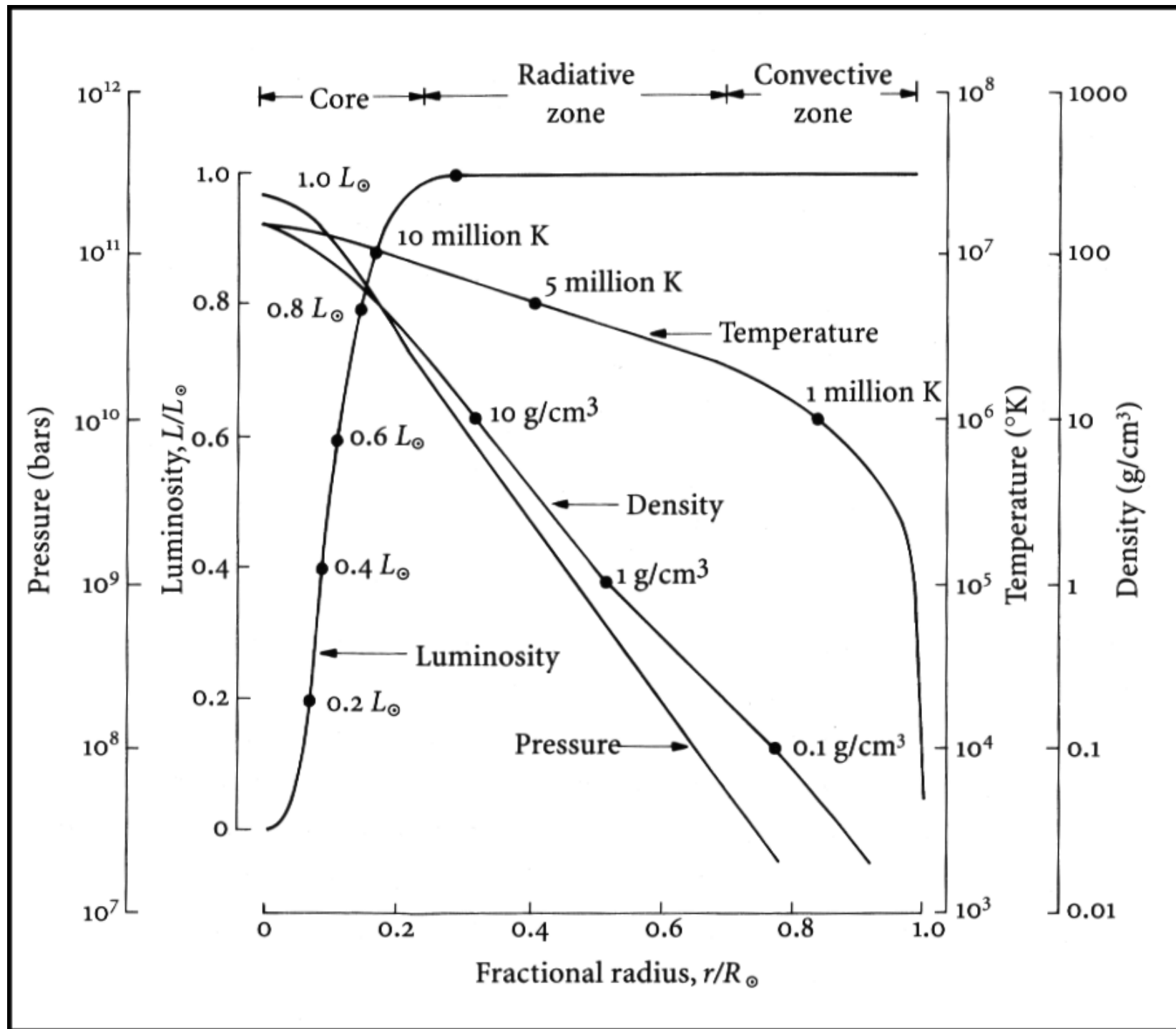


Figure 13.2 A cutaway figure showing the interior structure of the Sun. (a) Temperature, density, and pressure increase toward the center of the Sun. (b) Energy is generated in the Sun's core.





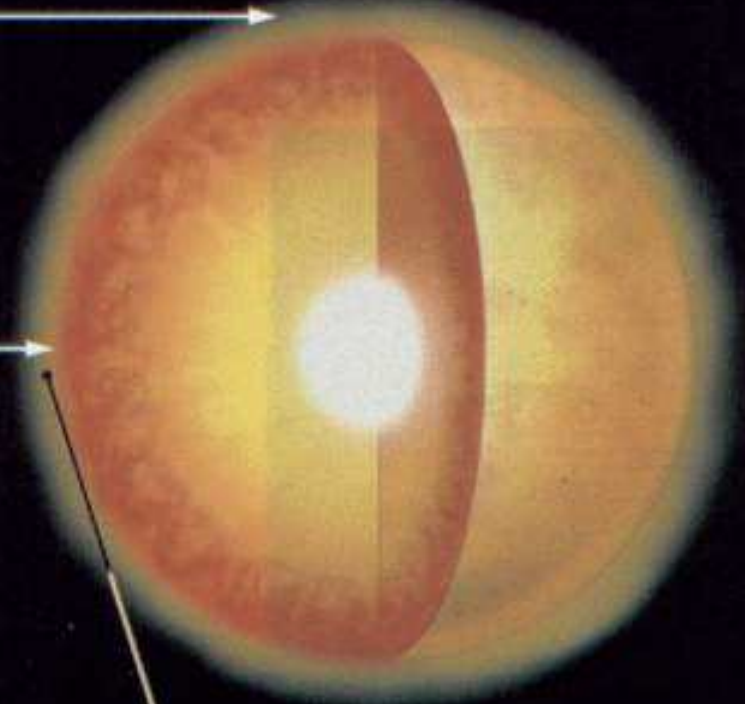
1 The Sun is "limb darkened."
It is fainter near its edge...

(a)



2 ...because near its edge we see
the Sun at a steep angle, and so do
not see deeply into its atmosphere.

(b)



3 Near its center we observe the surface
of the Sun face-on, and so see deeper
into hotter, brighter regions.

White Light



14 Apr 1980 04:48



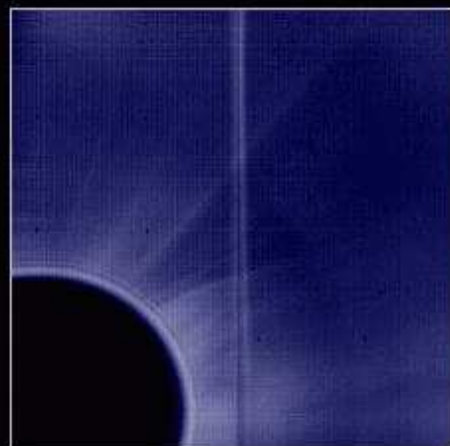
14 Apr 1980 05:44



14 Apr 1980 06:10



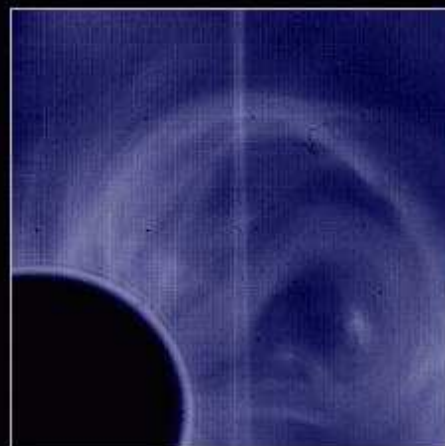
14 Apr 1980 07:09



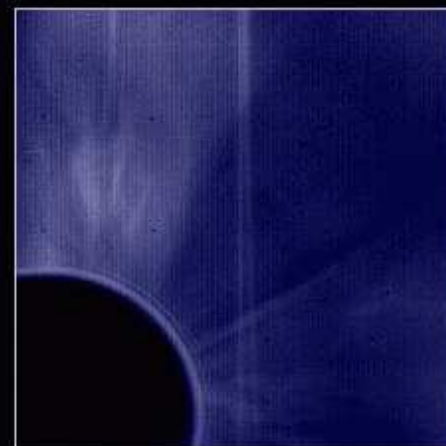
24 Oct 1989 15:23



24 Oct 1989 18:09



24 Oct 1989 18:25

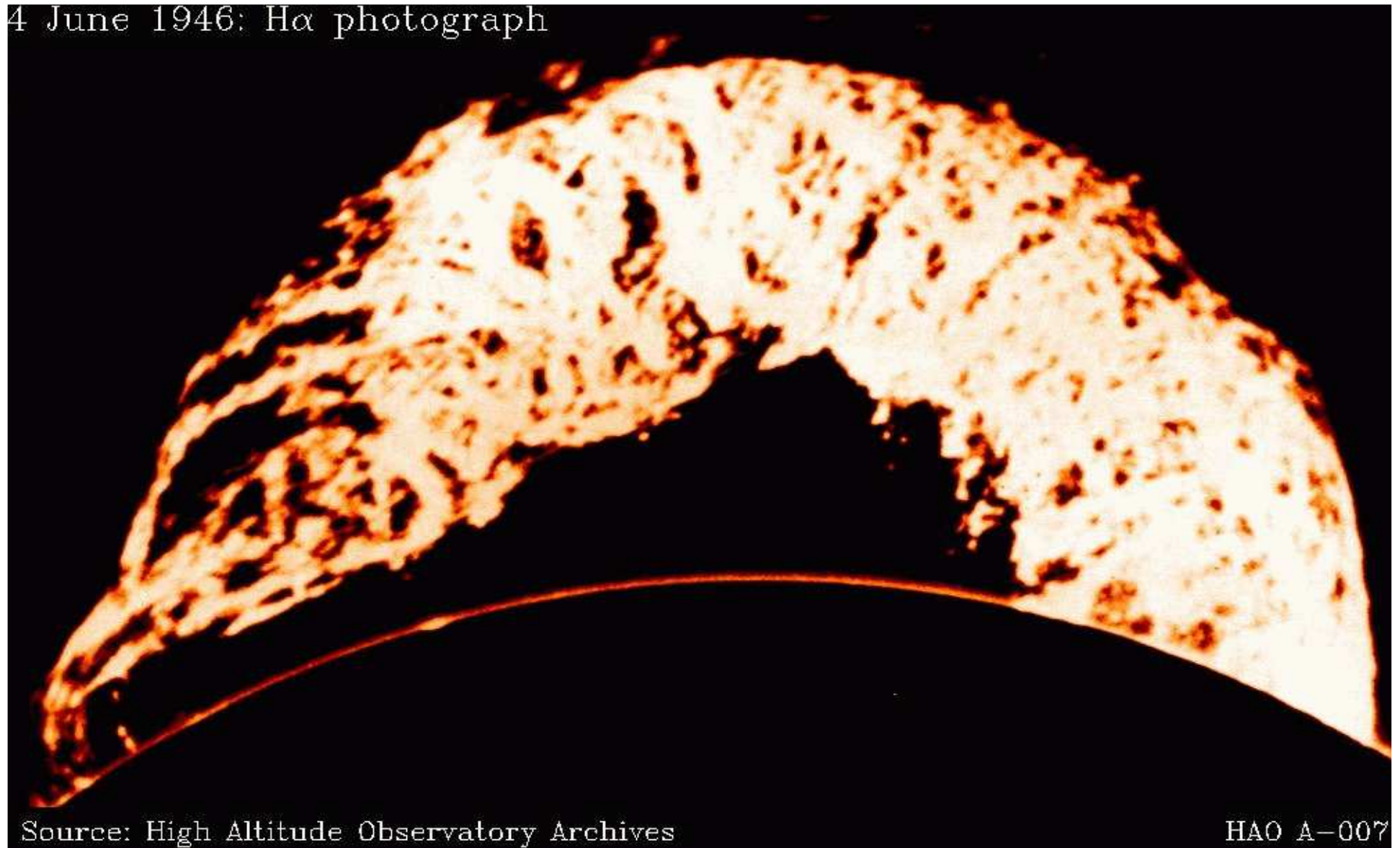


24 Oct 1989 19:15

Source: High Altitude Observatory/Solar Maximum Mission Archives

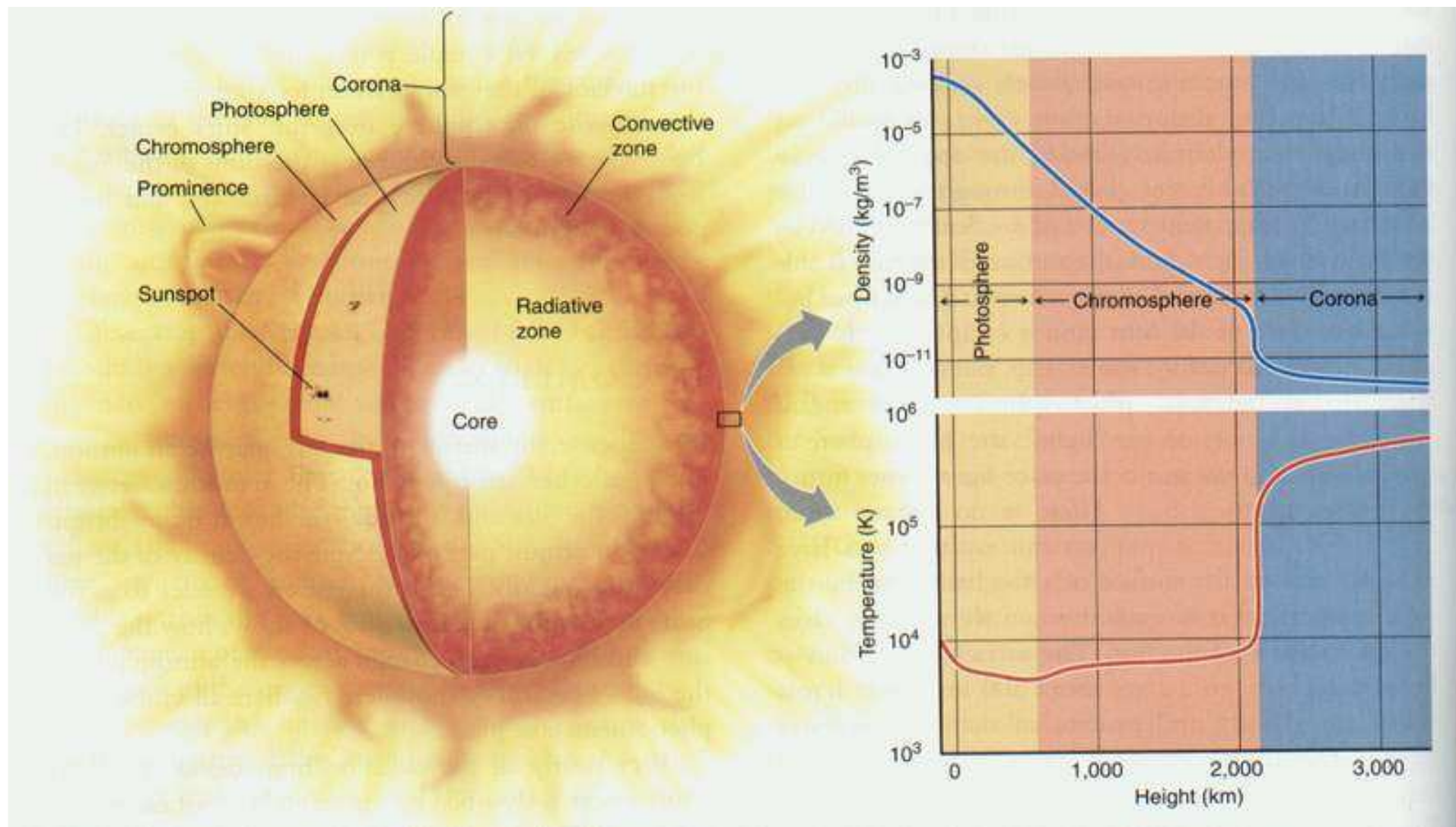
HAO A-014

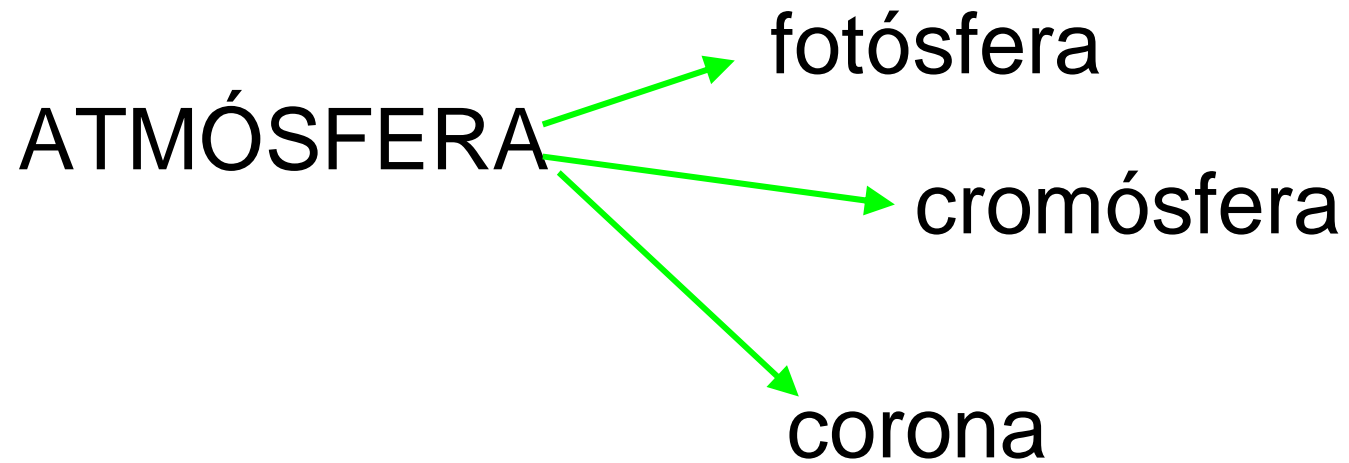
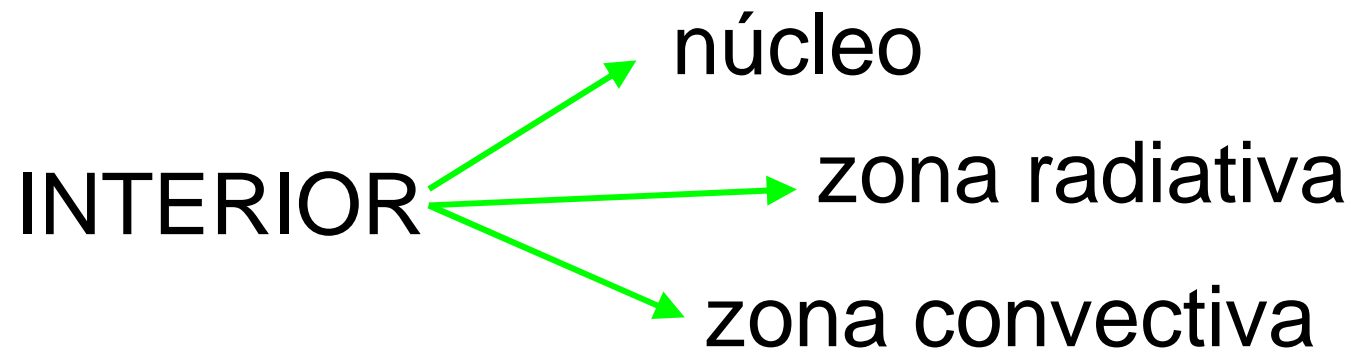
4 June 1946: H α photograph



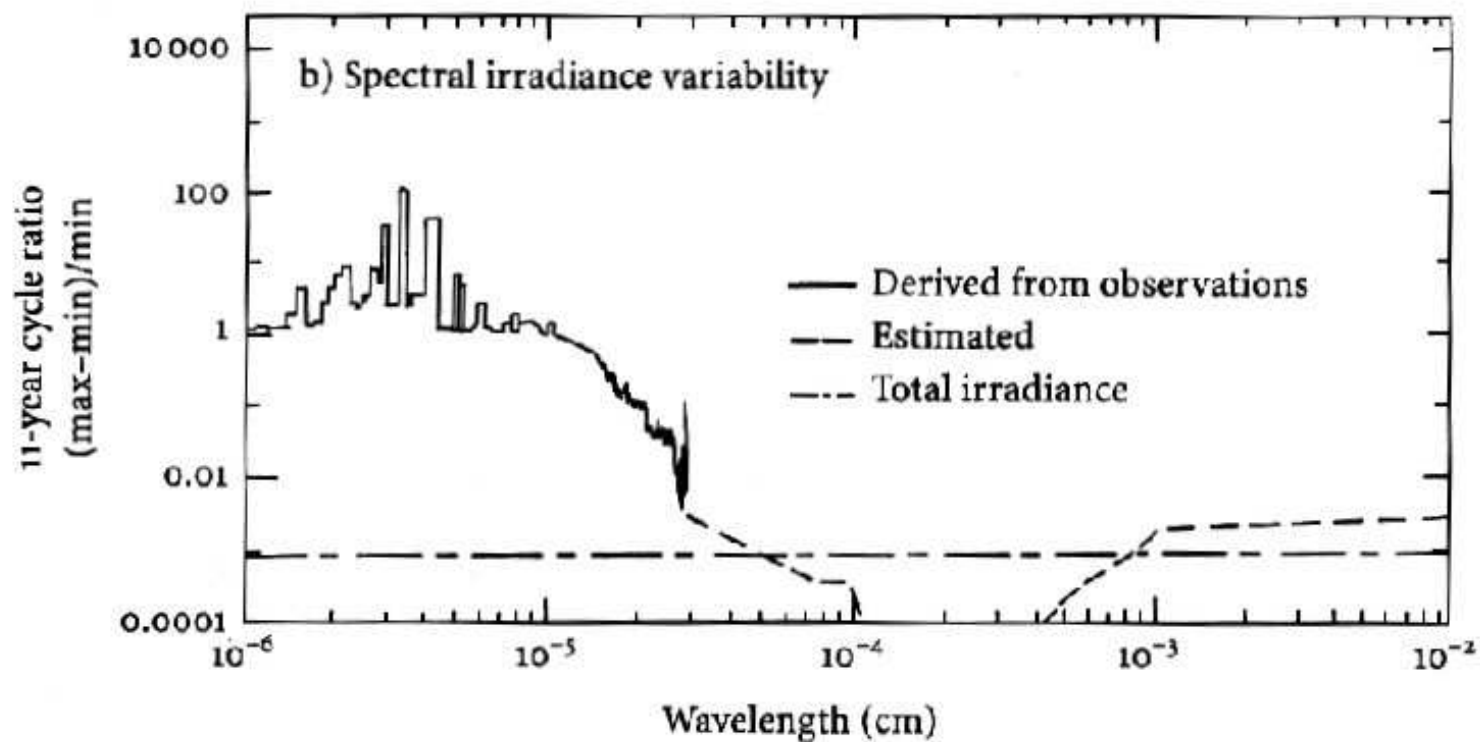
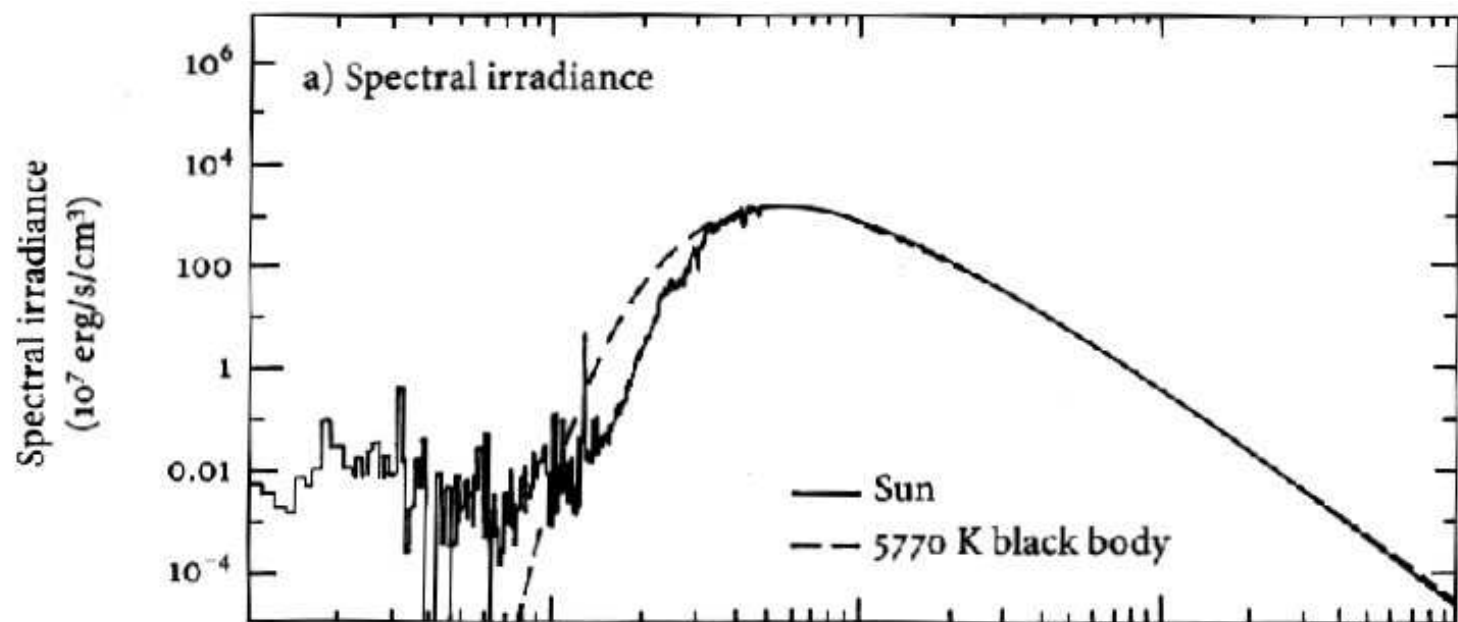
Source: High Altitude Observatory Archives

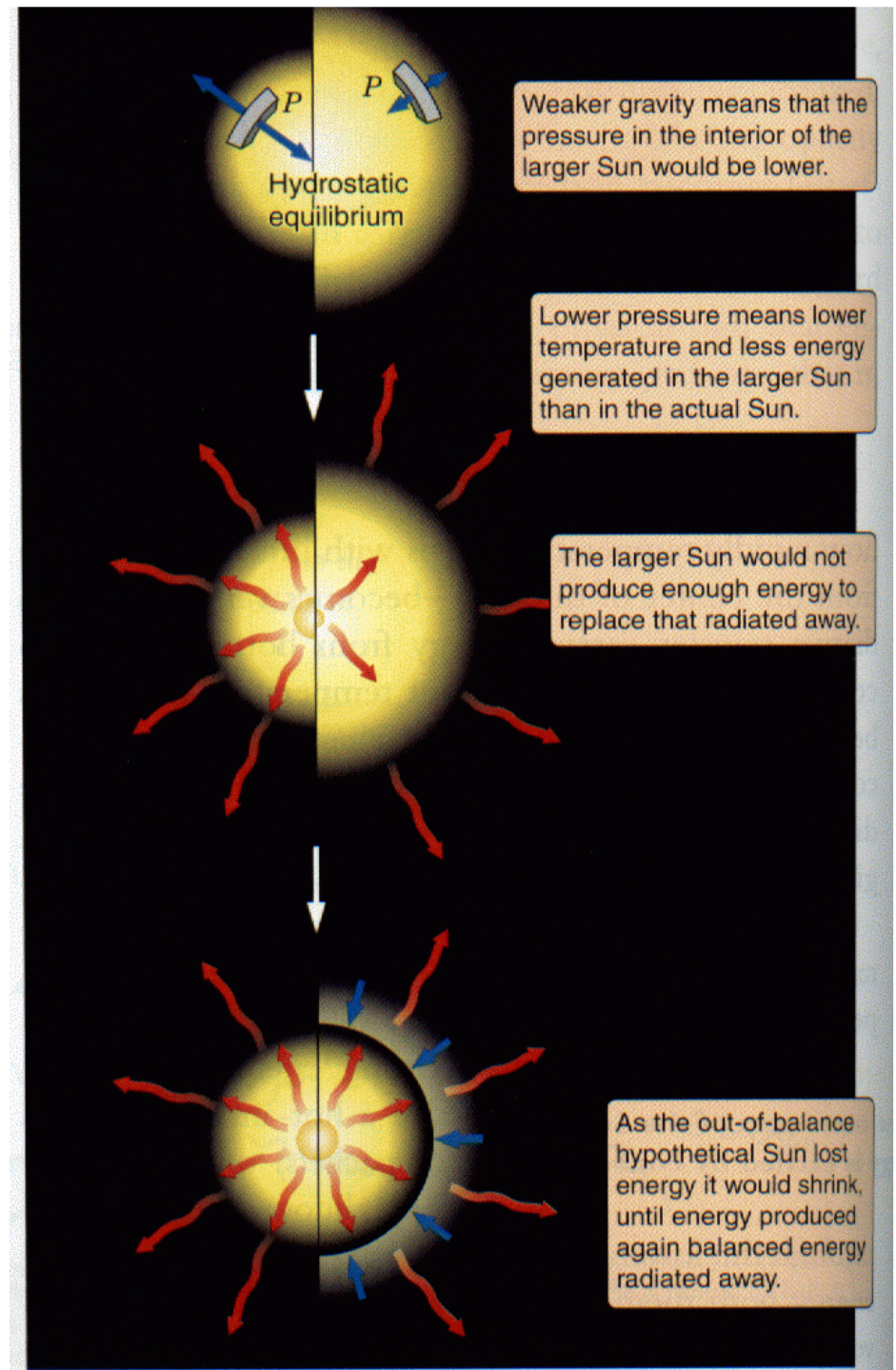
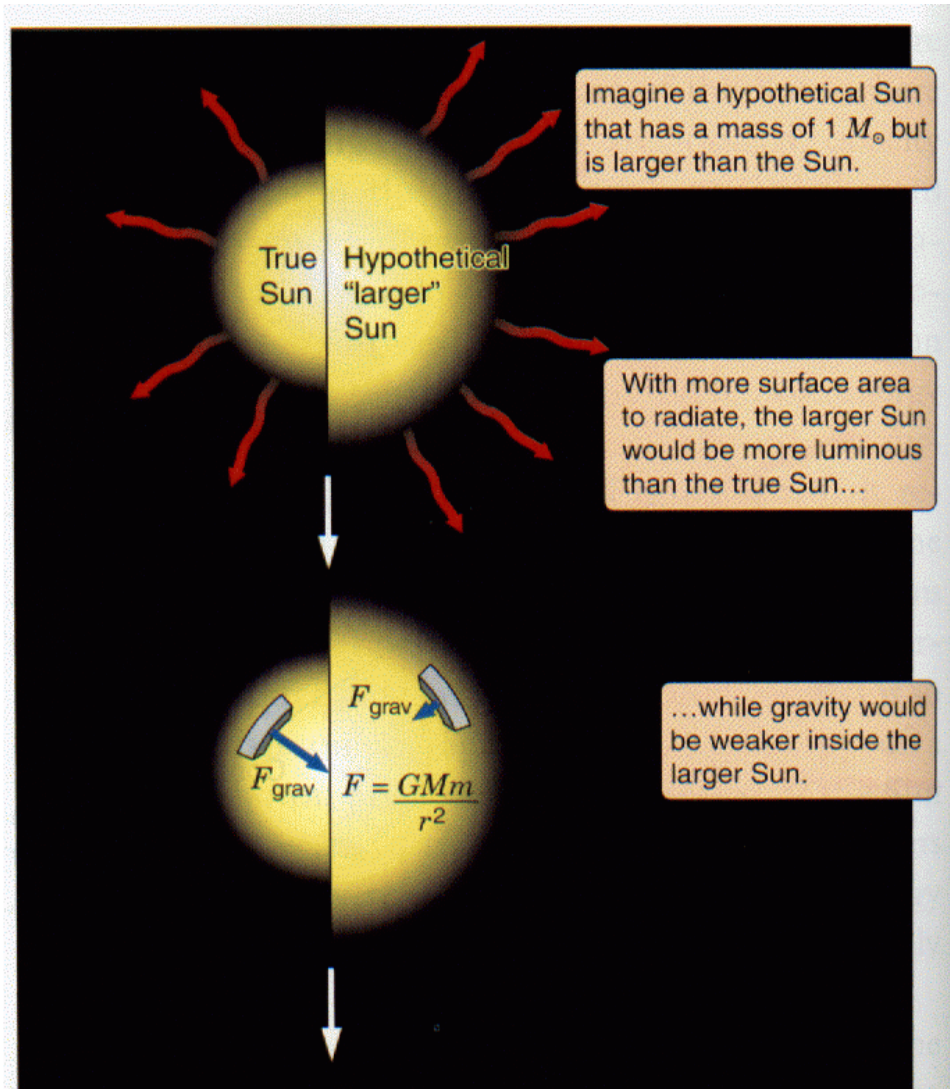
HAO A-007





VIENTO SOLAR





Condiciones en el centro

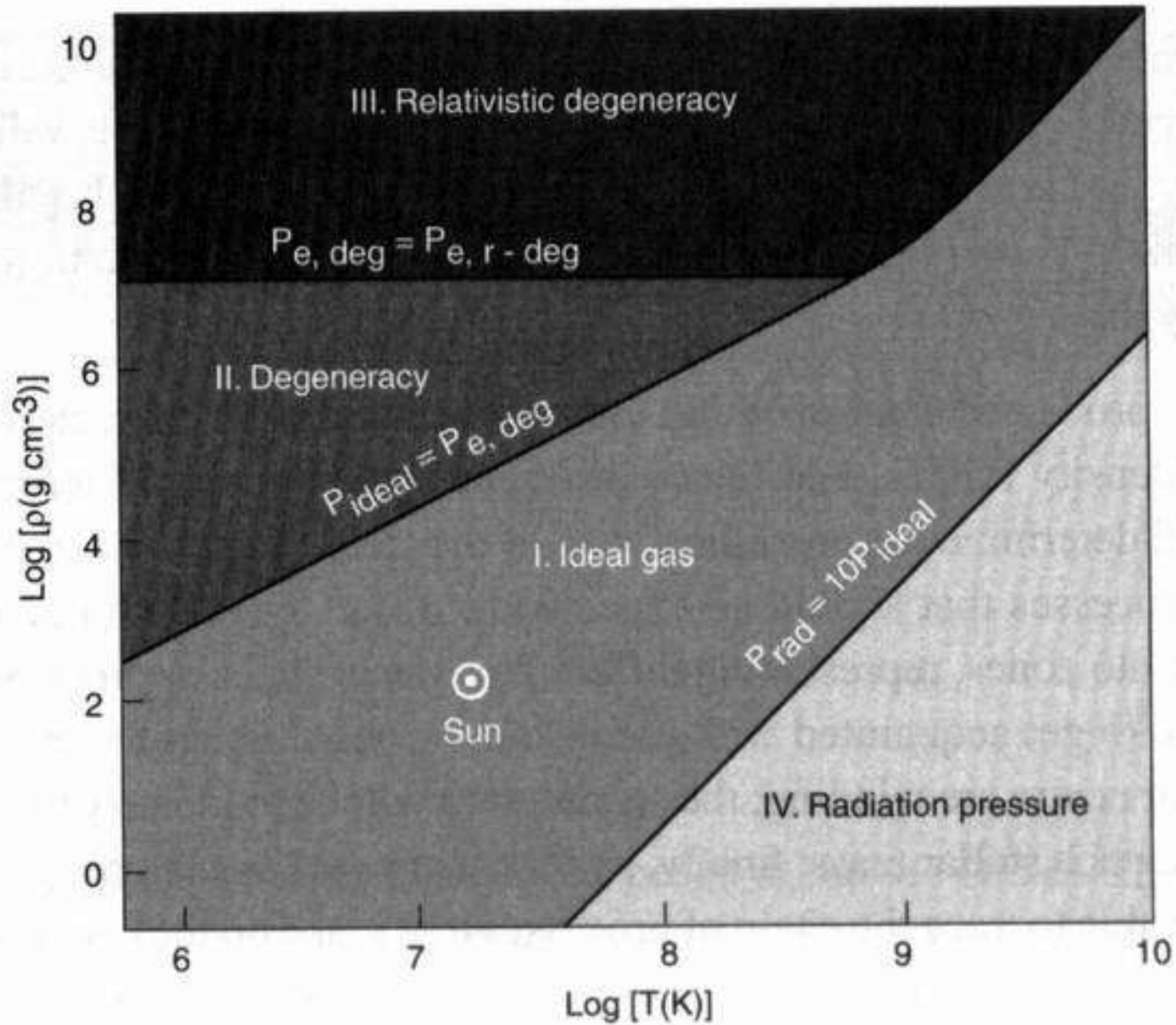


Figure 7.1 Mapping of the temperature-density diagram according to the equation of state

ENERGIA

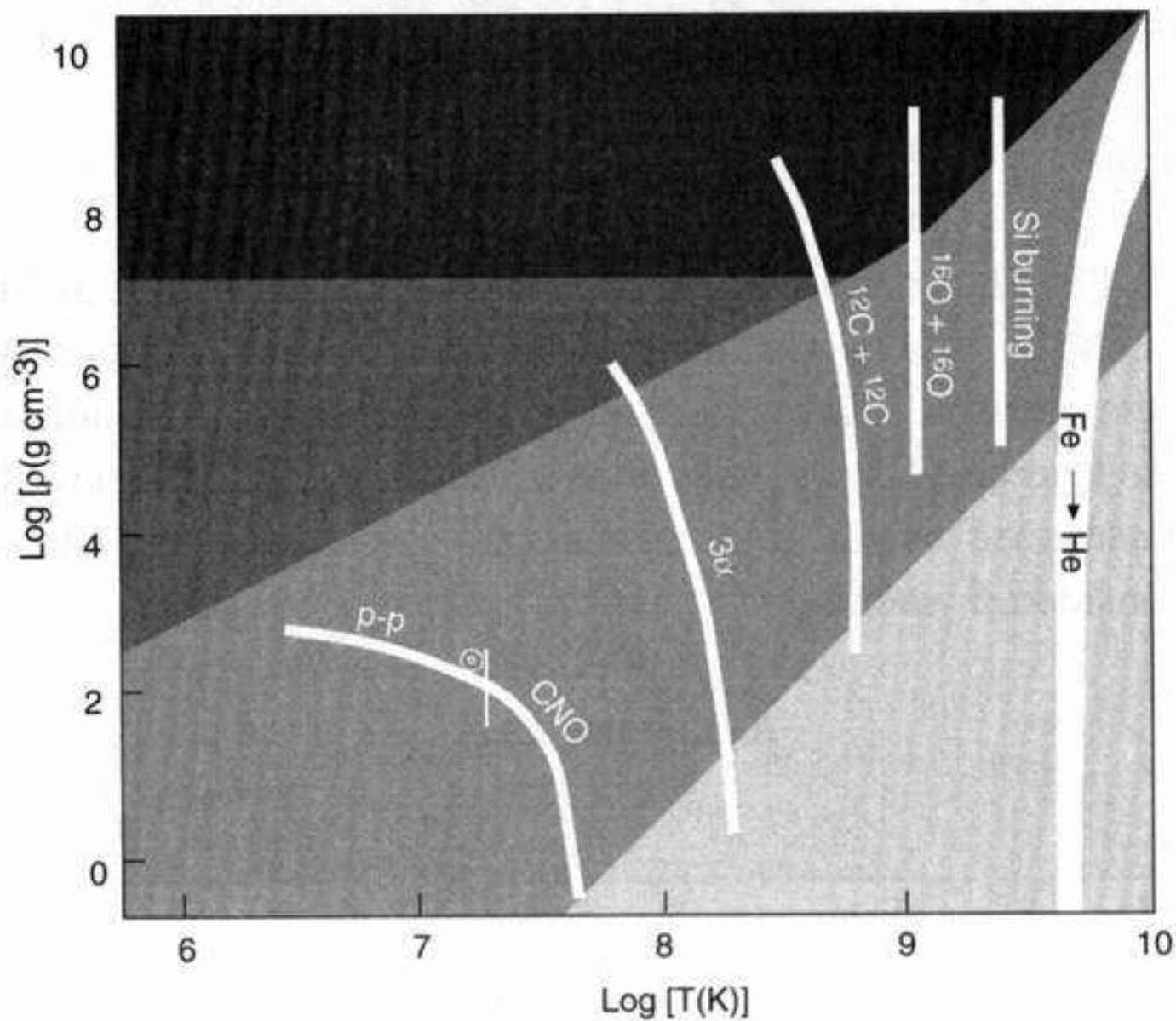


Figure 7.2 Mapping of the temperature-density diagram according to nuclear processes.

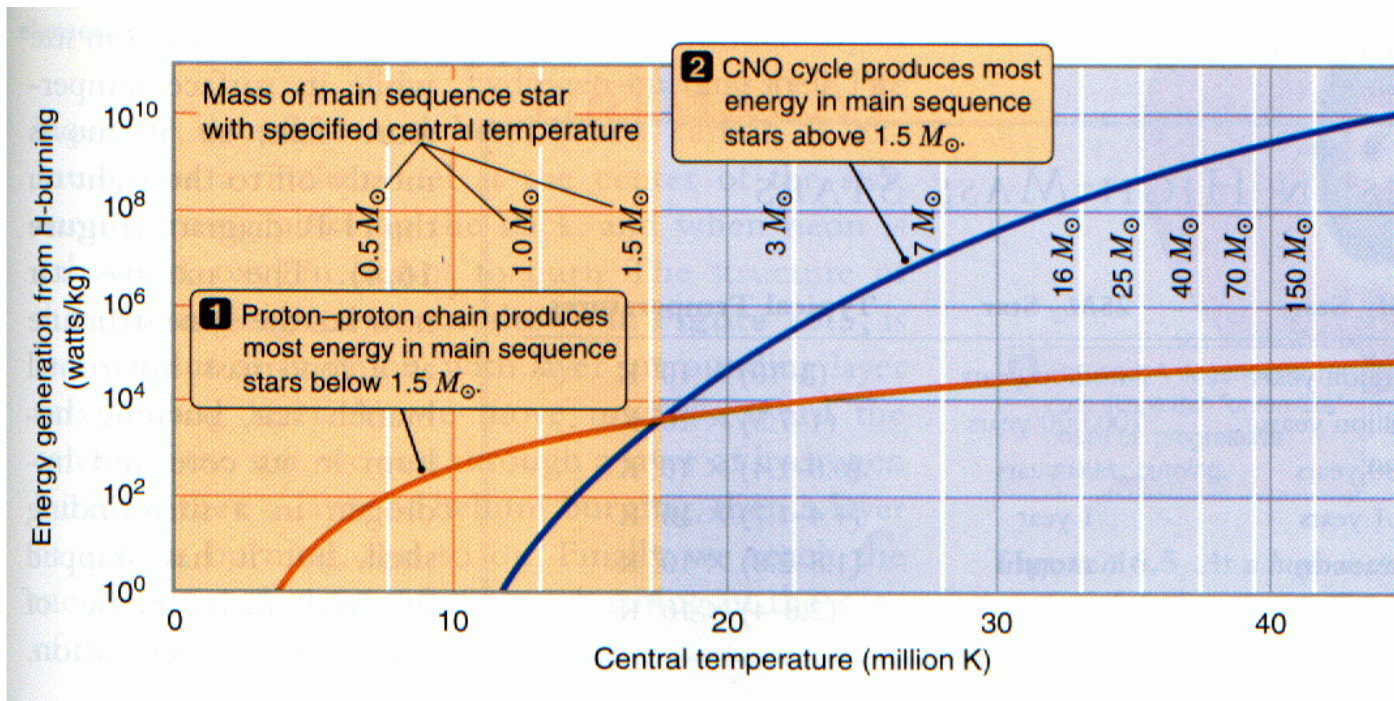
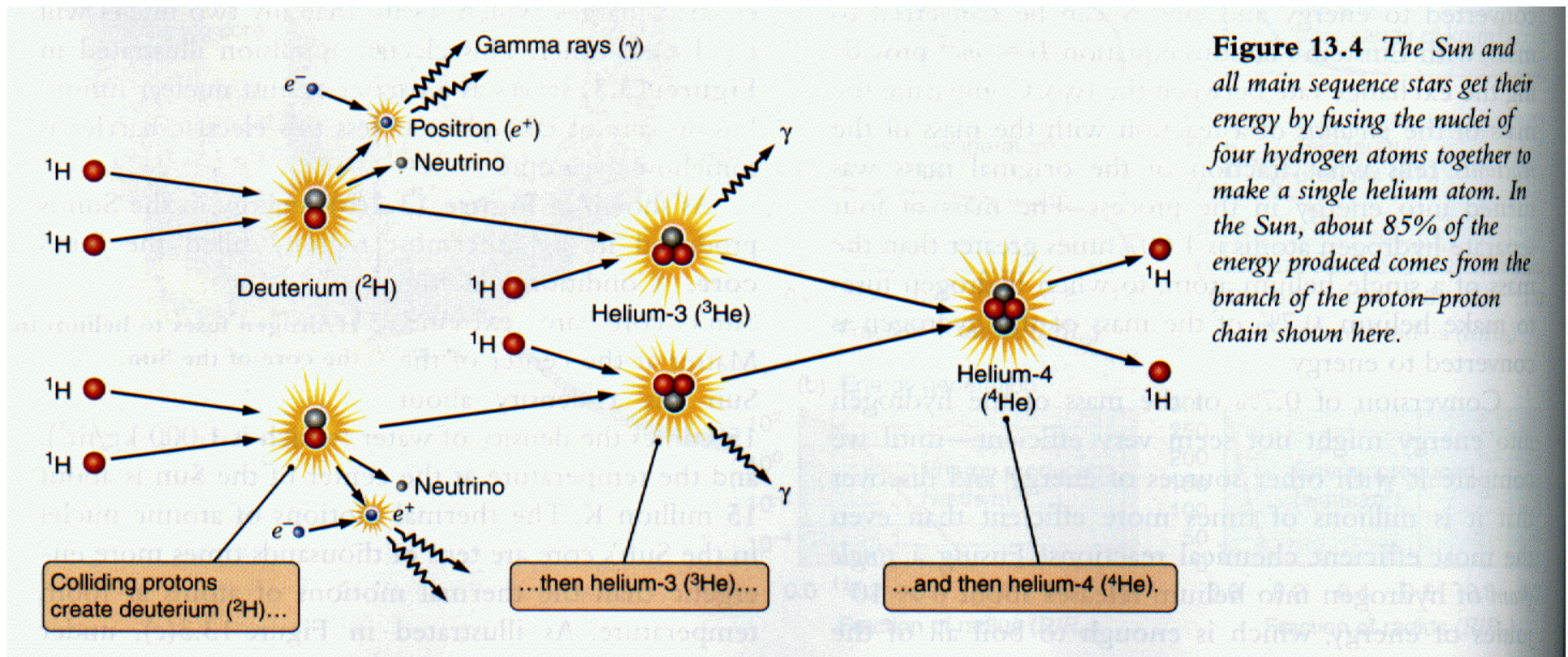


Figure 16.2 Plots of the rate of energy generation as a function of temperature for the proton-proton chain and the CNO cycle. At the higher central temperatures of stars more massive than $1.5 M_{\odot}$, it is the CNO cycle that more efficiently fuses hydrogen into helium.



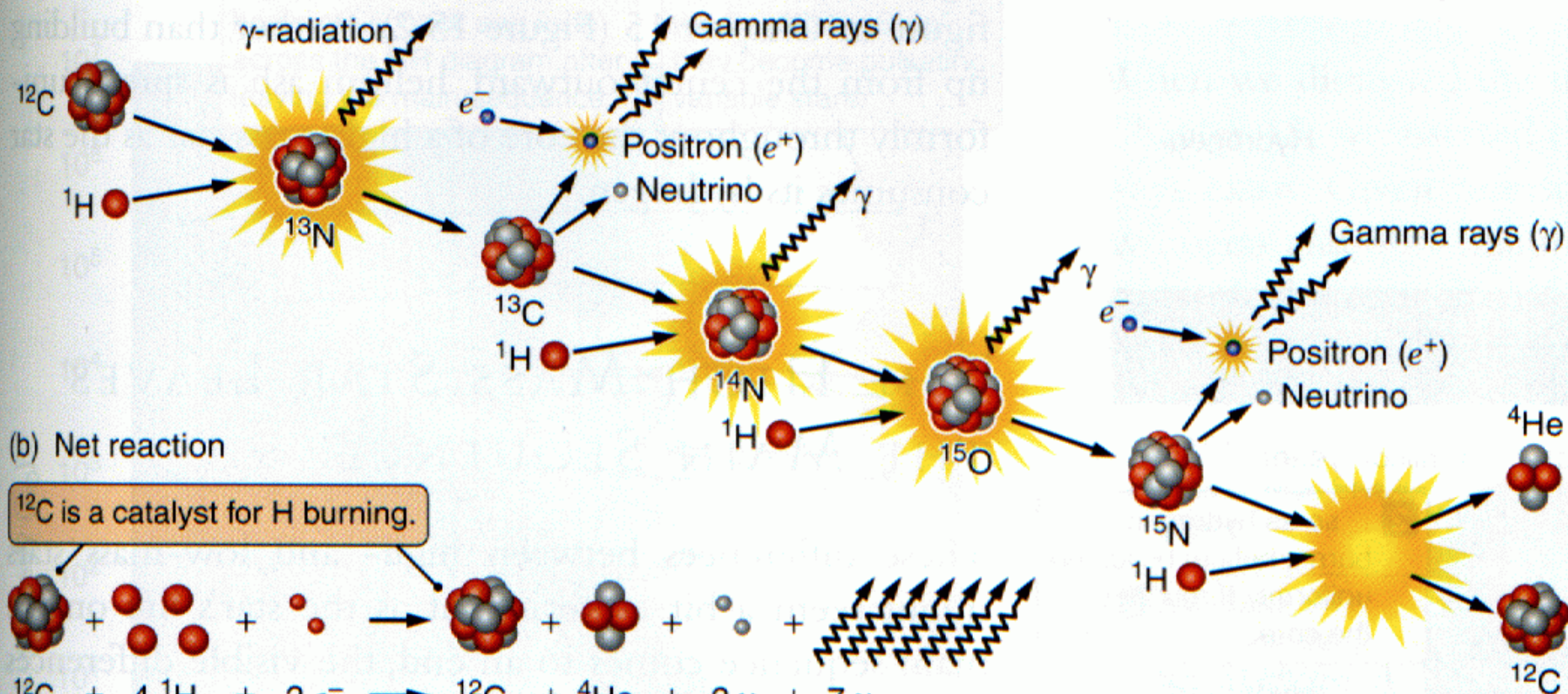
Fraccion de masa que se convierte en energia

$$\frac{\Delta m}{m(4H)} = 0.007$$

Energia generada

$$\mathcal{E} = \Delta m \times c^2$$

(a) CNO cycle



(b) Net reaction

^{12}C is a catalyst for H burning.

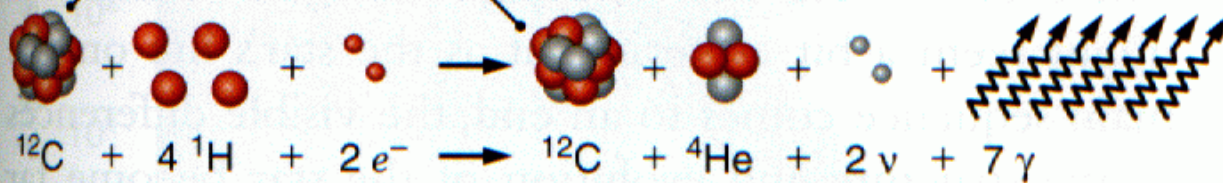
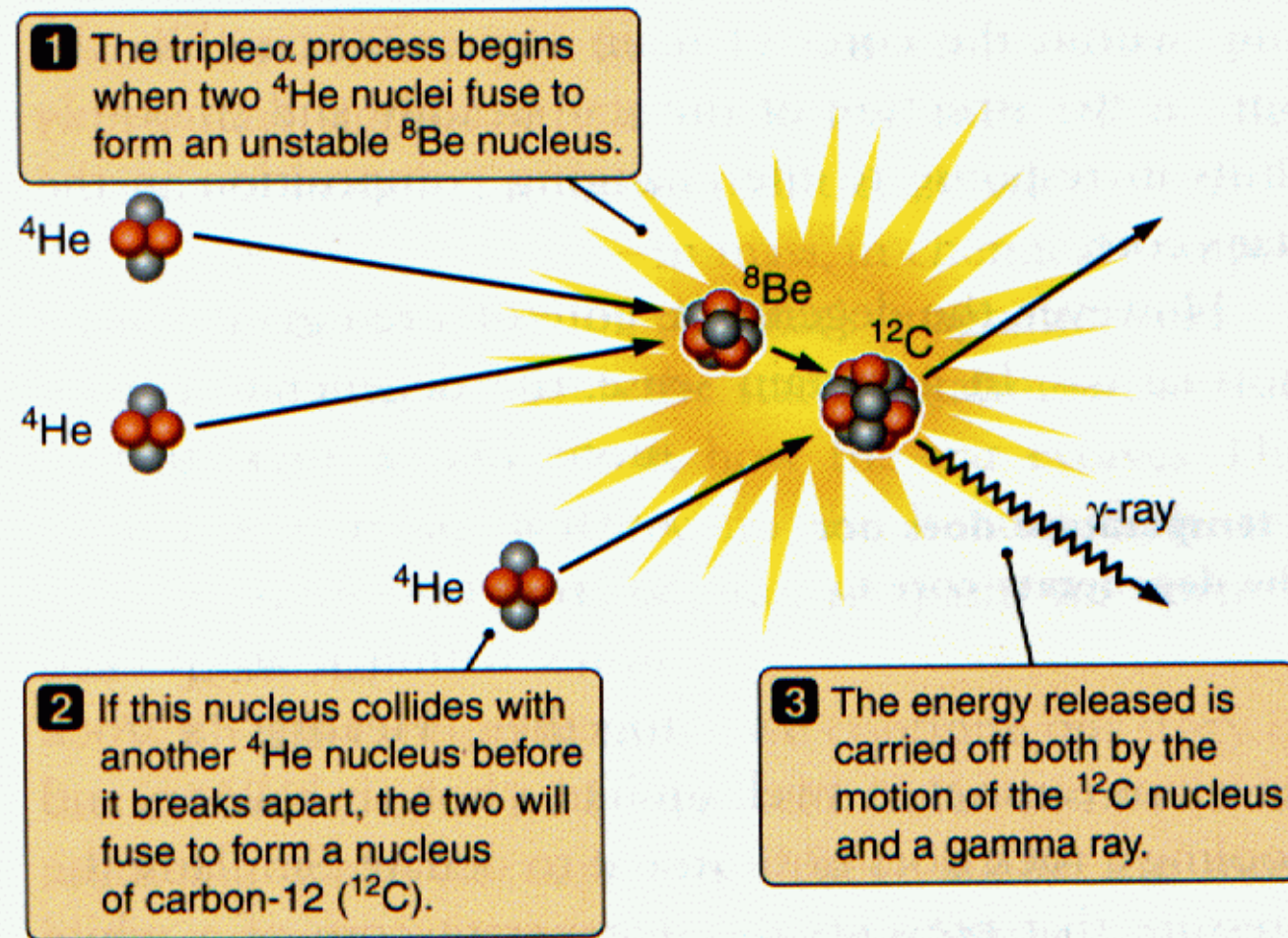


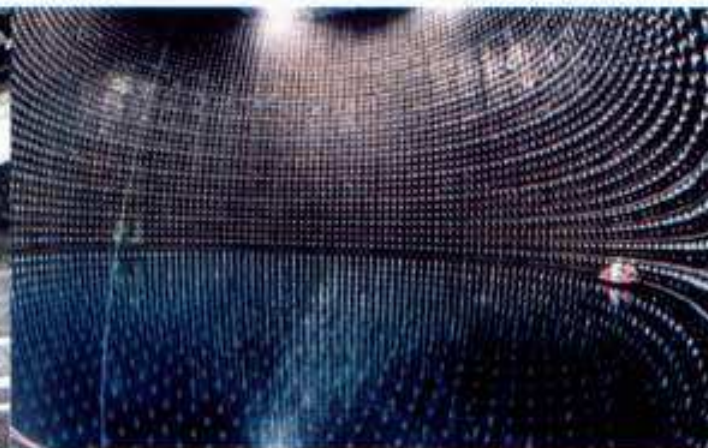
Figure 15.7 The triple-alpha processes: Two ${}^4\text{He}$ nuclei fuse to form an unstable ${}^8\text{Be}$ nucleus. If this nucleus collides with another ${}^4\text{He}$ nucleus before it breaks apart, the two will fuse to form a stable nucleus of carbon-12 (${}^{12}\text{C}$). The energy produced is carried off both by the motion of the ${}^{12}\text{C}$ nucleus and by a high-energy gamma ray emitted in the second step of the process.



(a)



(b)

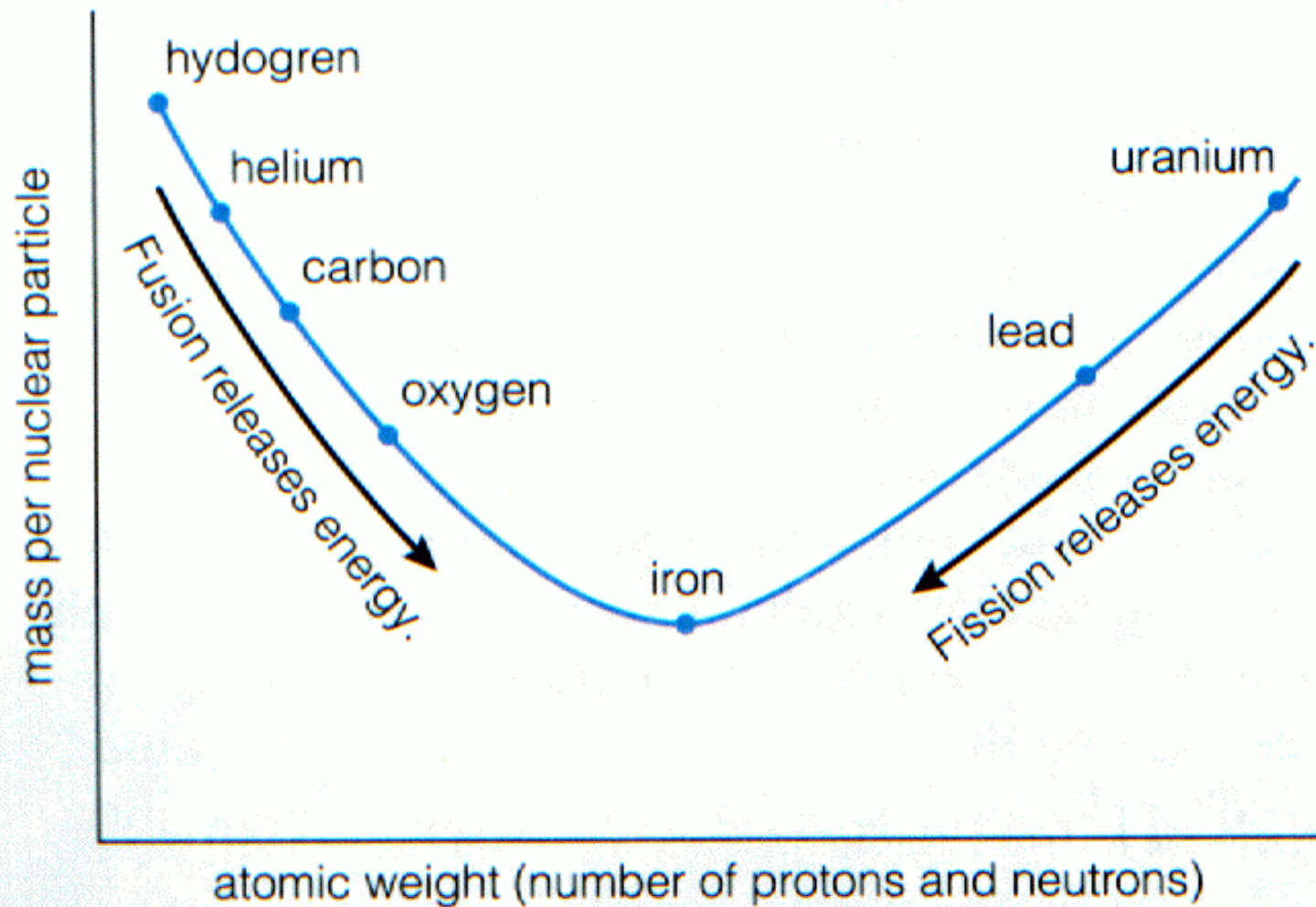


(c)



Figure 13.8 Neutrino “telescopes” do not look much like visible-light telescopes. (a) The Homestake neutrino detector is a 100,000-gallon tank of dry cleaning fluid located deep in a mine in South Dakota. (b) The Super Kamiokande detector (shown before it was completely filled) is a tank containing 50,000 tons of pure water surrounded by over 11,000 photomultiplier tubes that record flashes of light from reactions within the tank. (c) A map of the flash of light from a single neutrino detected by the Super Kamiokande detector.

FIGURE 16.18 Overall, the average mass per nuclear particle declines from hydrogen to iron and then increases. Selected nuclei are labeled to provide reference points. (This graph shows the most general trends only; a more detailed graph would show numerous up-and-down bumps superimposed on the general trend.)



Stellar fusion processes^a

PP I chain	PP II chain	PP III chain
$p^+ + p^+ \rightarrow {}^2_1\text{H} + e^+ + \nu_e$ ${}^2_1\text{H} + p^+ \rightarrow {}^3_2\text{He} + \gamma$ ${}^3_2\text{He} + {}^3_2\text{He} \rightarrow {}^4_2\text{He} + 2p^+$	$p^+ + p^+ \rightarrow {}^2_1\text{H} + e^+ + \nu_e$ ${}^2_1\text{H} + p^+ \rightarrow {}^3_2\text{He} + \gamma$ ${}^3_2\text{He} + {}^4_2\text{He} \rightarrow {}^7_4\text{Be} + \gamma$ ${}^7_4\text{Be} + e^- \rightarrow {}^7_3\text{Li} + \nu_e$ ${}^7_3\text{Li} + p^+ \rightarrow 2{}^4_2\text{He}$	$p^+ + p^+ \rightarrow {}^2_1\text{H} + e^+ + \nu_e$ ${}^2_1\text{H} + p^+ \rightarrow {}^3_2\text{He} + \gamma$ ${}^3_2\text{He} + {}^4_2\text{He} \rightarrow {}^7_4\text{Be} + \gamma$ ${}^7_4\text{Be} + p^+ \rightarrow {}^8_5\text{B} + \gamma$ ${}^8_5\text{B} \rightarrow {}^8_4\text{Be} + e^+ + \nu_e$ ${}^8_4\text{Be} \rightarrow 2{}^4_2\text{He}$
CNO cycle	triple- α process	
${}^{12}_6\text{C} + p^+ \rightarrow {}^{13}_7\text{N} + \gamma$ ${}^{13}_7\text{N} \rightarrow {}^{13}_6\text{C} + e^+ + \nu_e$ ${}^{13}_6\text{C} + p^+ \rightarrow {}^{14}_7\text{N} + \gamma$ ${}^{14}_7\text{N} + p^+ \rightarrow {}^{15}_8\text{O} + \gamma$ ${}^{15}_8\text{O} \rightarrow {}^{15}_7\text{N} + e^+ + \nu_e$ ${}^{15}_7\text{N} + p^+ \rightarrow {}^{12}_6\text{C} + {}^4_2\text{He}$	${}^4_2\text{He} + {}^4_2\text{He} \rightleftharpoons {}^8_4\text{Be} + \gamma$ ${}^8_4\text{Be} + {}^4_2\text{He} \rightleftharpoons {}^{12}_6\text{C}^*$ ${}^{12}_6\text{C}^* \rightarrow {}^{12}_6\text{C} + \gamma$	γ photon p^+ proton e^+ positron e^- electron ν_e electron neutrino

^aAll species are taken as fully ionised.

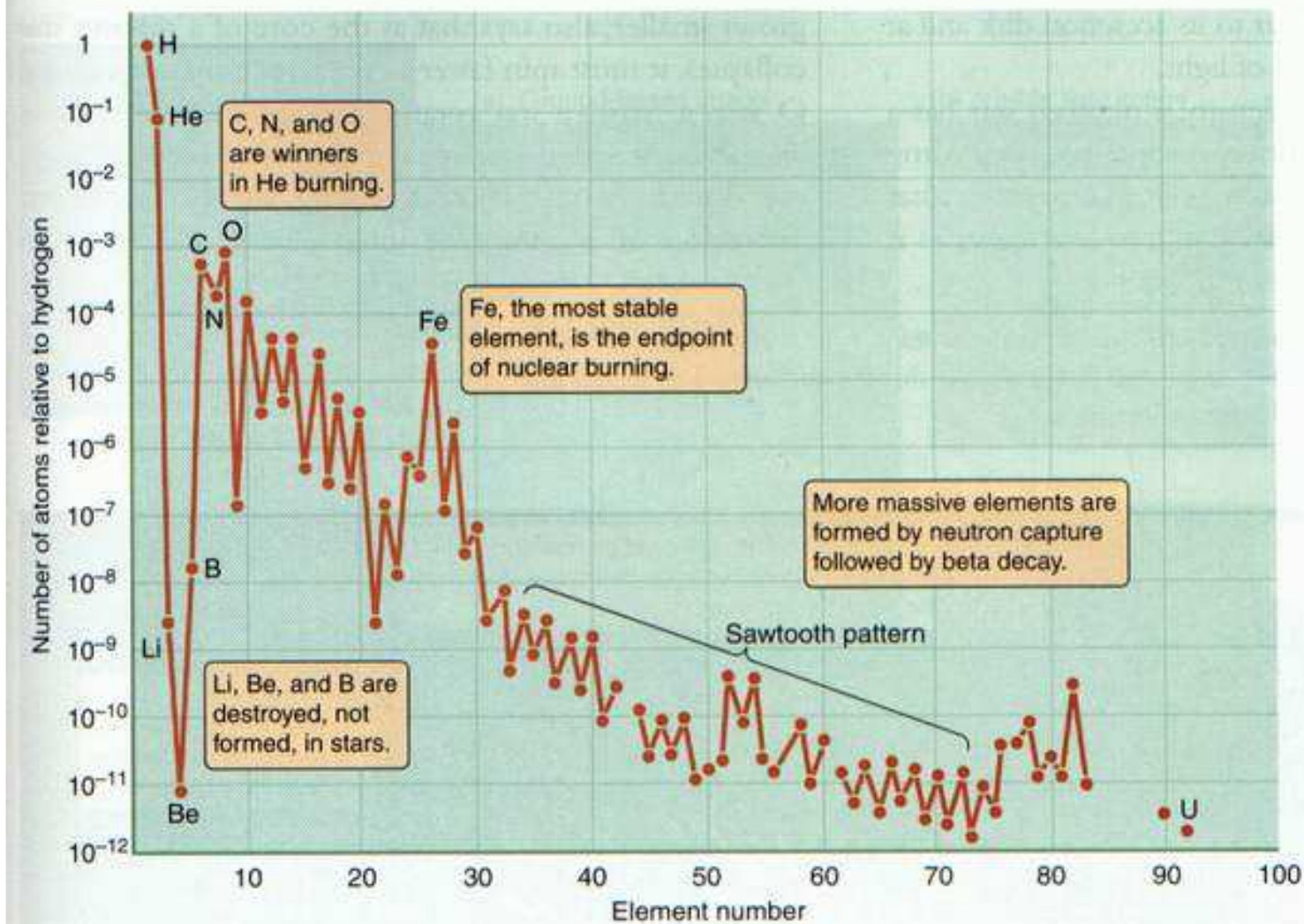


Figure 16.12 The relative abundances of different elements on Earth are plotted against the mass of the nucleus. This pattern can be understood as a result of the process of nucleosynthesis in stars.

Li, Be, B